Geophysical Journal International

Geophys. J. Int. (2013) **194,** 1295–1301
Advance Access publication 2013 June 3

doi: 10.1093/gji/ggt189

Kinematics of rotating panels of E–W faults in the San Andreas system: what can we tell from geodesy?

J. P. Platt and T. W. Becker

Department of Earth Sciences, University of Southern California, Los Angeles, CA 90089-0742*, USA. E-mail: jplatt@usc.edu*

Accepted 2013 May 8. Received 2013 May 6; in original form 2012 October 2

SUMMARY

Sets of E- to NE-trending sinistral and/or reverse faults occur within the San Andreas system, and are associated with palaeomagnetic evidence for clockwise vertical-axis rotations. These structures cut across the trend of active dextral faults, posing questions as to how displacement is transferred across them. Geodetic data show that they lie within an overall dextral shear field, but the data are commonly interpreted to indicate little or no slip, nor any significant rate of rotation. We model these structures as rotating by bookshelf slip in a dextral shear field, and show that a combination of sinistral slip and rotation can produce the observed velocity field. This allows prediction of rates of slip, rotation, fault-parallel extension and fault-normal shortening within the panel. We use this method to calculate the kinematics of the central segment of the Garlock Fault, which cuts across the eastern California shear zone at a high angle. We obtain a sinistral slip rate of 6.1 ± 1.1 mm yr^{-1}, comparable to geological evidence, but higher than most previous geodetic estimates, and a rotation rate of $4.0 \pm 0.7^\circ$ Myr^{-1} clockwise. The western Transverse Ranges transect a similar shear zone in coastal and offshore California, but at an angle of only 40°. As a result, the faults, which were sinistral when they were at a higher angle to the shear zone, have been reactivated in a dextral sense at a low rate, and the rate of rotation of the panel has decreased from its long-term rate of $\sim 5^\circ$ to $1.6^\circ \pm 0.2^\circ$ Myr^{-1} clockwise. These results help to resolve some of the apparent discrepancies between geological and geodetic slip-rate estimates, and provide an enhanced understanding of the mechanics of intracontinental transform systems.

Key words: Continental margins: transform; Continental tectonics: strike-slip and transform; Dynamics and mechanics of faulting; Fractures and faults; Kinematics of crustal and mantle deformation; Crustal structure; North America.

1 INTRODUCTION

In several areas within the San Andreas Transform system, the predominantly NW-trending arrays of dextral faults are interrupted by E- to NE-trending faults with geological evidence for sinistral slip (Fig. 1). These areas include the western Transverse Ranges (WTR) and the Garlock Fault (discussed in more detail later), the eastern Transverse Ranges (Carter *et al.* 1987; Spinler *et al.* 2010), a panel of E-trending sinistral faults in the NE Mojave Desert (Schermer *et al.* 1996), and another near Reno, Nevada (Cashman & Fontaine 2000). All of these regions are associated with significant palaeomagnetically determined vertical-axis rotations.

The E-trending sinistral faults are in general not cut or deflected by dextral structures, except locally at their terminations; and in most cases the dextral faults either terminate before they reach the sinistral structures (Oskin & Iriondo 2004), or they bend and appear to merge with them (Onderdonk 2005). Only the San Andreas Fault (SAF) itself clearly cross-cuts the E-trending structures. Geodetic data, however, suggest that 7–8 mm yr^{-1} of dextral slip is being transferred across the WTR from the central California Coast Ranges into the southern California Borderland (e.g. McCaffrey 2005; Meade & Hager 2005; Platt & Becker 2010). Similarly, 10–11 mm yr^{-1} of dextral slip in the eastern California shear zone (ECSZ, McClusky *et al.* 2001; Bennett *et al.* 2003) is being transferred southwards across the Garlock Fault into the Mojave Desert (Savage *et al.* 2001). The velocity distributions from both these regions suggest that dextral shear is transmitted across the sinistral faults without interruption or deflection, but the geodetic data have been interpreted to indicate that the sinistral faults are not slipping at a significant rate (e.g. Savage *et al.* 2001), or that the intervening crustal blocks are not rotating (e.g. McCaffrey 2005). There is, therefore, a long-standing problem about how the dextral displacement expressed on the NW-trending dextral faults is transferred across the sinistral faults and fault panels.

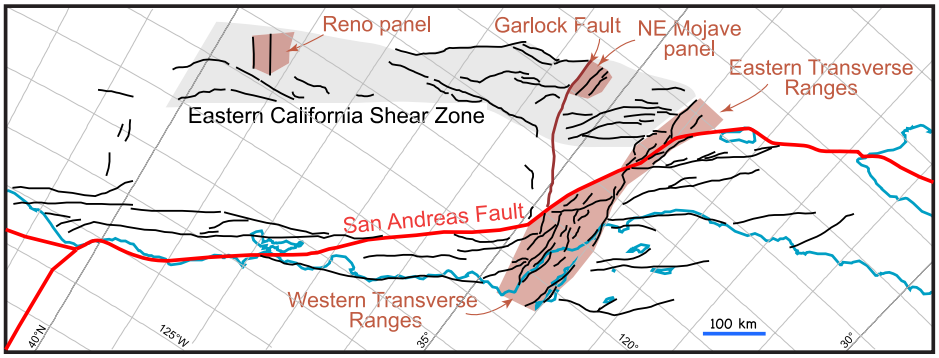

Figure 1. Map of active faults in California, plotted parallel to the Pacific–North American plate motion vector, showing panels of E–W trending sinistral faults (brown shade).

2 BOOKSHELF SLIP

A possible explanation for these cross-cutting faults and fault panels is that they formed by a process known as bookshelf slip (Fig. 2): a combination of sinistral shear on the faults, plus wholesale clockwise rotation of the faults and the surrounding rocks, is kinematically equivalent to distributed dextral shear parallel to the transform zone as a whole (e.g. Luyendyk *et al.* 1980; Cowan *et al.* 1986; Schermer *et al.* 1996). This process is most easily visualized if the sinistral faults are normal to the shear zone, as in that case no additional components of deformation are required. If the faults are oblique to the shear zone (i.e. if the angle $\alpha \neq 90^\circ$ in Fig. 2), there have to be additional components of deformation to maintain compatibility (McKenzie & Jackson 1983).

Previous analyses of this situation (e.g. Luyendyk *et al.* 1980; Cowan *et al.* 1986) have assumed that the fault blocks do not deform internally, in which case holes open up between the blocks, and there have to be components of motion of the bounding plates normal to the shear zone to accommodate the rotating blocks. At the scale of the lithosphere, this is unlikely to be realistic: plate motions

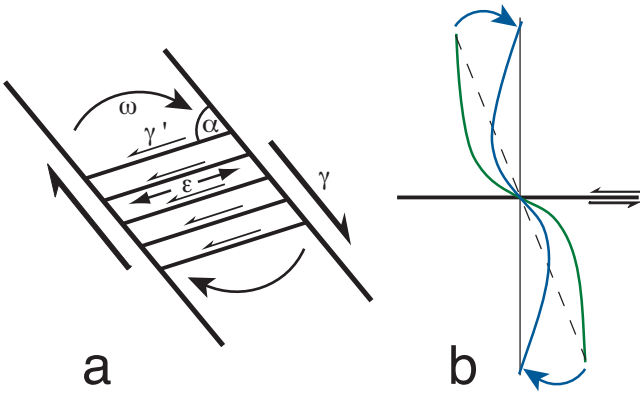

Figure 2. (a) Idealized model of a panel of sinistral faults undergoing bookshelf slip in a dextral shear system. The combination of sinistral slip (γ'), clockwise rotation (ω) and internal stretching of the fault blocks (ε) is equivalent to dextral shear (γ). (b) Residual elastic velocity profile across one of the sinistral faults. Green line shows schematically the interseismic velocity profile predicted by the elastic dislocation model for a sinistral fault. If the fault is rotating clockwise in a dextral shear zone, as in (a), the sinistral displacement is cancelled out, but the elastic velocity profile is rotated with the fault (blue line).

are unlikely to be dictated by small blocks in the boundary zone, and body forces will act to prevent large-scale gaps opening between the blocks. Luyendyk *et al.* (1980) do in fact show that sedimentary basins have formed in the WTR where these gaps would be expected, but the scale and depth of these basins are unlikely to lead to significant deviations from the assumption of strain compatibility. We assume here that the shear zone as a whole maintains a constant width, and that the deformation is horizontal plane strain and simple shear. Under those assumptions, the faults and fault blocks rotate and change length in the same way that lines would do in a continuously deforming material. Hence, if $\dot{\gamma}$ is the bulk rate of dextral shear, and α the angle of the oblique faults to the plane of bulk simple shear, the rate of shear on the oblique fault array is $\dot{\gamma}' = \dot{\gamma} \cos 2\alpha$, the rate of rotation of the faults and fault blocks is $\dot{\omega} = \dot{\gamma}(1 - \cos 2\alpha)/2$ and the fault blocks have to stretch or shorten internally at a rate $\dot{e} = \dot{\gamma} \sin 2\alpha/2$ to maintain compatibility with their surroundings (Fig. 2a). If the bulk deformation is horizontal plane strain, there will also be a component of shortening or extension normal to the fault blocks, at a rate $\dot{e} = -\dot{\gamma} \sin 2\alpha/2$. Deformation is likely to be heterogeneous on the scale of the individual blocks, but these relationships provide an approximate description that is applicable at the scale of the panels as a whole. On the boundaries of the rotating zone, there will be local patterns of rotation and slip on minor faults that transfer displacement from the NW-trending dextral faults to the E-trending sinistral faults.

An important prediction of the bookshelf slip model is that the rates of slip and rotation on the oblique faults will be at a maximum when they are at 90° to the shear zone. Rates of slip and rotation decrease as α decreases, but rates of stretching of the fault blocks increase. As α decreases past 45°, the slip rate drops to zero and then reverses sense, and the stretching rate reaches a maximum. For $\alpha <$ 45°, the faults become dextral, and the rotation rate progressively decreases. These predictions differ from those of the floating block model described by Lamb (1987), and applied to the eastern Transverse Ranges by Giorgis *et al.* (2004), in which the blocks rotate continuously at a rate related to their aspect ratio, their orientation and the vorticity of flow in the shear zone.

In this study, we investigate the velocity field adjacent to the Garlock Fault and the WTR to see if these structures can be interpreted in terms of the bookshelf slip model, and we determine the rates of rotation and related strain that would be predicted by the transfer of dextral shear across these structures. We chose these two examples because the density of long-term geodetic stations is high enough, and the velocity gradients around the sinistral faults are large enough, that flexural effects associated with slip on the faults

may be detectable. For the other examples, slip rates on the faults are of the order of 1–2 mm yr^{-1}, which is too slow for us to detect the second-order signal we are looking for.

3 GARLOCK FAULT

The Garlock Fault is a somewhat unusual example of the phenomenon we are investigating here, as it consists of a single sinistral fault cutting across the ECSZ at a high angle. We chose it for analysis because it has the highest rates of slip and rotation predicted by the bookshelf model of any of the E–W trending fault systems in the San Andreas system, and hence it gives us the best chance of detecting these processes from geodetic data. The fault comprises three distinct sectors:

(1) Garlock/San Andreas intersection to the Sierran eastern front. This sector trends 55° E of N, and lies west of the ECSZ. The geodetic velocity field in this area is dominated by the accumulation of elastic strain on the SAF. Little permanent dextral shear strain is being transmitted across this sector, and the rotation rate is likely to be small.

(2) Sierran front to Death Valley fault zone. This sector trends ∼75°E of N; it cuts across the region of highest dextral shear strain rate within the ECSZ, and hence is likely to have a high rate of rotation.

(3) Death Valley fault zone eastward. This sector is largely hidden beneath recent sediment (Davis & Burchfiel 1973). The rate of dextral shear strain parallel to the ECSZ decreases eastwards, and the slip rate on the Garlock presumably decreases towards its hidden eastern termination.

The Garlock Fault has been interpreted as a transfer structure, accommodating westward motion of the Sierra Nevada block, caused by E–W extension on normal faults in the Great Basin relative to the non-extending Mojave Block to the south (Davis & Burchfiel 1973). Some part of the present-day slip on the Garlock may be a result of ongoing Basin and Range extension, but this is difficult to evaluate, as present-day normal faulting north of the Garlock Fault is NW-directed, and appears to be related to dextral shear in the ECSZ. Slip rates on the Garlock Fault estimated from offset geological features are in the range 4–11 mm yr^{-1}, and mainly come from the central sector of the fault (McGill *et al.* 2009). Our analysis focuses on the central 100 km, which appears to have the highest slip rate, and is most clearly affected by dextral shear in the ECSZ.

3.1 Method of analysis

We base our calculations on the velocities in a region around the central segment of the Garlock Fault (Fig. 3a). We argue that within this region, roughly defined by a circle 100 km in diameter (blue circle in Fig. 3a), slip on the NW-trending dextral faults is converted into a combination of sinistral slip on the Garlock Fault and vertical-axis clockwise rotation. All geodetic velocities are published Global Positioning System (GPS) estimates and based on our merger of the EarthScope Plate Boundary Observatory (PBO) solutions and the compilation of Kreemer & Hammond (2007), as used by Platt & Becker (2010). However, the data are here updated to use the most recent, 2011 August 1, release of the PBO network velocities (as of 2013 March). The PBO solution is used with doubled velocity uncertainties, for reasons discussed by Platt & Becker (2010), in the original, North America fixed reference frame.

We can calculate rotations and strain rates related to local deformation from the spatial gradients in the velocity field, but we first have to correct for sphericity-related gradients associated with the local angular velocity of the area around the Euler pole describing its motion relative to North America. If the angular distance from the Euler pole is θ, then the gradient in the velocity V normal to the great circle through the Euler pole $\partial V/\partial\theta = V/\tan\theta$. Correcting for these gradients is not straightforward, as part of the local angular velocity will result from the internal vorticity produced by the deformation. We therefore assume to a first approximation that the deformation is related to Pacific–North America plate motion. We determine the average velocity of the area being analysed relative to North America, and express that as a fraction of the total velocity of the Pacific Plate for that area (26 per cent in the case of the Garlock Fault), using the geodetically determined Euler pole of Meade & Hager (2005). For each individual velocity vector, we subtract 26 per cent of the Pacific Plate motion at its location. This correction has two advantages. (1) The remaining velocities are those that are directly related to deformation in the area. (2) The correction removes 26 per cent of the sphericity-related velocity gradient of the Pacific Plate, which is a reasonable estimate of that gradient for the area around the Garlock Fault.

The corrected GPS solutions are shown on a Mercator projection in Fig. 3(a); the vectors coloured red and green are the ones used in our analysis. Because the regional velocity has been removed, the noisiness of the data is apparent, but examination of the data shows that the primary signal is the dextral shear gradient across the ECSZ.

Figs 3(b) and (c) show normal and tangential components of motion along a profile approximating the Garlock Fault, north (green) and south (red) of the fault. Velocity gradients are related to the tensor components of strain rate and rotation, so the gradient in the fault-normal velocity, which averages 7.45×10^{-8} radians yr^{-1} (4.3° Myr^{-1}) north and south of the fault, represents the current rate of rotation of the fault and its surroundings relative to the North American Plate, and the gradient in the tangential velocity represents the rate of extension parallel to the fault (2.54×10^{-8} yr^{-1}).

Using a swath from the same data set across the region of Fig. 3, Platt & Becker (2010) estimated the strain rate across the ECSZ at 8.66×10^{-8} yr^{-1}, or 8.1 mm yr^{-1} across the 94-km wide central section. This rate of dextral shear strain should cause the central section of the Garlock Fault to rotate at 7.65×10^{-8} radians yr^{-1}, which compares well with the fault-normal velocity gradient shown in Fig. 3(b).

For the purposes of calculating long-term rates of rotation and slip, we need to remove transient components of the velocity field. Based on the velocity profiles and slip rates estimated by Platt & Becker (2010), we attribute ∼1 mm yr^{-1} of the velocity difference south of the Garlock Fault to far-field elastic strain related to the SAF; north of the Garlock this effect is not measurable. Transient post-seismic displacement rates related to the 1999 Hector Mine earthquake had dropped to <0.17 mm yr^{-1} near the Garlock Fault by 2006 (Freed *et al.* 2012), and can therefore be neglected. Post-seismic viscoelastic relaxation related to earthquakes throughout the western part of the North American Plate as far away as the Cascadia margin and the Juan de Fuca rise may also contribute to the overall velocity field. Pollitz *et al.* (2008), for example, calculate velocities of around 5 mm yr^{-1} in the vicinity of the Garlock Fault as a result of post-seismic relaxation from the 1700 Cascadia margin earthquake. Our analysis largely removes these velocities along with the rest of the average velocity field, to focus on the velocity gradients. Velocity gradients associated with his estimates are

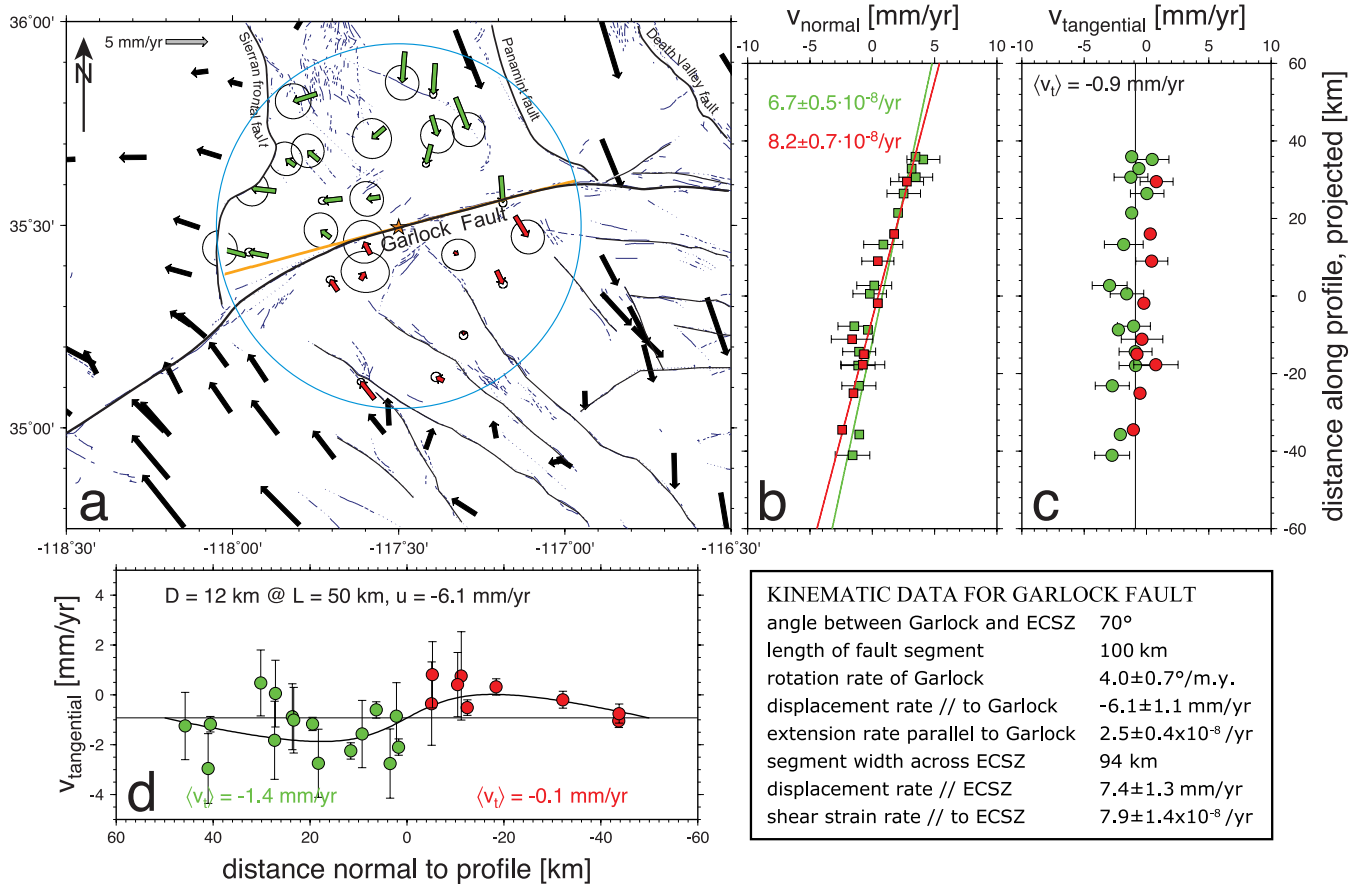

Figure 3. (a) Velocity field around the central section of the Garlock Fault. Red and green vectors were used in this analysis. Blue circle indicates the approximate region within which dextral shear is accommodated by sinistral slip on the Garlock Fault plus clockwise rotation. (b) Fault-normal velocities projected onto a line (gold) approximating the fault trajectory, in a direction parallel to the motion on the ECSZ (azimuth 145°). The gradient along the fault reflects the rate of rotation of the fault and surrounding rocks. (c) Transverse velocities projected as in (b). The gradient reflects the rate of extension parallel to the fault. (d) Transverse velocity distribution across the fault, with best-fitting arctan profile for the calculated slip rate of 6.1 mm yr^{-1} (see text for discussion).

$<4 \times 10^{-9}$ yr^{-1}, which is less than the uncertainties on our estimates of local gradients. Another potential source of disturbance is the 1872 *M*7.6 Lone Pine earthquake in Owens Valley, ∼150 km north of the Garlock Fault. We have calculated the post-seismic relaxation following that earthquake using a simple two-layer model with a 30-km elastic plate overlying a viscoelastic half-space, using the formulation of Barbot & Fialko (2010) and the source parameters of Pollitz *et al.* (2008). Given a range of typical Maxwell times, we estimate the gradients to be $\sim 2 \times 10^{-9}$ yr^{-1}, and therefore likewise negligible for our analysis. Hence, the only correction we have made in addition to the sphericity correction is to subtract 0.5 ± 0.5 mm yr^{-1} from our displacement rate estimate for the central section of the ECSZ, to account for the effect of the SAF.

We use the resulting corrected shear strain rate (7.9×10^{-8} yr^{-1}), to calculate the rate of sinistral slip on the Garlock Fault (6.1 ± 1.1 mm yr^{-1}), the rate of clockwise rotation of the fault and its surroundings ($4.0 \pm 0.7°$ Myr^{-1}), and the rate of extension parallel to the fault, using the relationships summarized in Section 2. These rates are summarized in the panel at the bottom of Fig. 3, and we discuss them in comparison to other geological and geodetic estimates later in the paper.

The variation in tangential velocities normal to the fault is shown in Fig. 3(d). The mean values on each side of the fault show a difference of ∼1.3 mm yr^{-1}, and the change occurs fairly rapidly across the fault. We suggest that this difference may reflect the interseismic elastic velocity profile related to long-term sinistral slip on the locked Garlock Fault, as illustrated in Fig. 2(b). The long-term slip rate itself is not apparent from the geodetic data, because the transverse velocities are cancelled out by the clockwise rotation of the whole system. We have inverted the velocity distribution for the locking depth, using a simple elastic dislocation model (Savage & Burford 1973). We assume a slip rate of 6.1 mm yr^{-1}, and a radius of 50 km for the rotating domain, which gives a best-fitting locking depth of 13 km. This is consistent with estimates for the locking depth of faults in California generally (e.g. Becker *et al.* 2005; Meade & Hager 2005). This interpretation is not unique, however, as the signal is only just detectable over the noise level in the data. An alternative interpretation, for example, is that there is ∼1 mm yr^{-1} of sinistral creep on the fault.

4 WTR

The WTR is a panel of E–W trending reverse and sinistral faults at an average angle of 40° to the plate motion vector, extending west from the region of the Big Bend in the SAF. A total of 8–9 mm yr^{-1} of dextral motion is transferred from the Inner Borderland across the WTR into the Coast Ranges (Platt & Becker 2010). This zone of dextral shear progressively narrows from south to north across the WTR; it is asymmetric, with the rate of shear

strain intensifying eastwards; and the zone is deflected westwards adjacent to the Big Bend, with a trend varying from 306° to 318°. Velocities near the eastern boundary of the shear zone are strongly influenced by elastic strain build-up on the SAF. These factors all complicate the analysis, which was carried out in the same way as for the Garlock Fault (Fig. 4). For the purposes of the analysis, we omitted the region within 30 km of the SAF, in which elastic effects of the fault are strongest, and considered a zone 118 km wide (measured normal to the SAF) trending parallel to the central sector of the SAF (318°). This zone corresponds to a 184-km long section of the WTR, indicated in Fig. 4.

The red and green vectors in Fig. 4 show the normal components of velocity on either side of a line extending from Point Conception to the Simi Hills. The spread in the fault-normal component of the velocities across the transect shown in Fig. 4(b) reflects convergence normal to the WTR: this increases eastwards to as much as 5 mm yr^{-1}. Much of this convergence reflects reverse motion on the faults due to oblique transfer of displacement from dextral faults in the inner Borderland into the Salinia Block (Platt & Becker 2010). This additional component of normal motion exaggerates the velocity gradient north of the line of the profile and increases the dispersion of the data. We therefore use the velocity gradient to the south of our profile line, which avoids most of the reverse faulting, but we assign a larger uncertainty. The gradient in the fault-normal velocities along the transect reflects the rate of rotation of the WTR, and the gradient in the tangential velocities (Fig. 4c) reflects extensional strain rate parallel to the WTR.

The fault-normal velocity gradient corresponds to a dextral shear strain in the Borderland of $7.7 \pm 0.5 \times 10^{-8}$ yr^{-1} parallel to the San Andreas transform, equivalent to a dextral displacement rate of 9.2 ± 0.6 mm yr^{-1}, which agrees well with the estimate by Platt & Becker (2010). We attribute 1.0 ± 0.3 mm yr^{-1} of this velocity difference to elastic strain build-up on the SAF. The remainder gives a long-term (geological) rate of dextral shear strain of $6.9 \pm 0.7 \times 10^{-8}$ yr^{-1} across the WTR. From this, we calculate a cumulative slip rate of 1.2 ± 0.1 mm yr^{-1} on the faults of the WTR in a dextral sense (this assumes the shear strain is distributed over a zone 100-km wide normal to the WTR, see Fig. 4a), a clockwise rotation rate of $1.6 \pm 0.2°$ Myr^{-1}, and a rate of stretching parallel to the trend of the WTR of $3.4 \pm 0.4 \times 10^{-8}$ yr^{-1}. This is equivalent to 6.0 ± 0.7 mm yr^{-1} extension along the 184 km length of the WTR. Our calculated rates are summarized in the panel at the bottom of Fig. 4.

The faults of the WTR are generally considered to be sinistral, with variable reverse components of motion (e.g. Bird 2009). Our analysis predicts that the current rate of strike-slip is very slow, but is dextral overall at a cumulative rate of 1.2 ± 0.2 mm yr^{-1} across all the faults. This apparent discrepancy is a result of the history of progressive clockwise rotation of the faults: when they were at a higher angle to the SAF they were sinistral, but once they had been

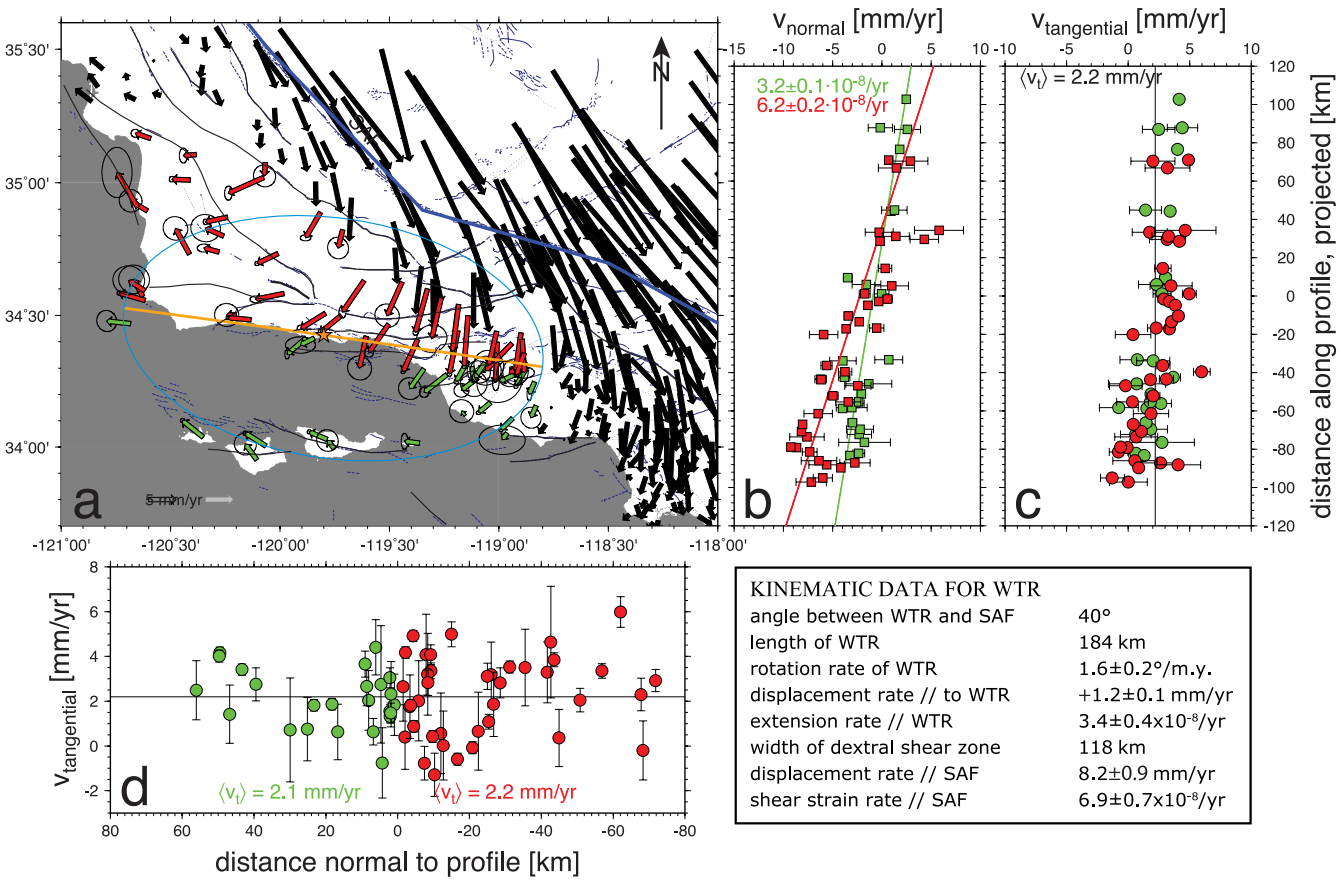

Figure 4. (a) Velocity field around the Western Transverse Ranges (WTR). Red and green vectors were used in this analysis. Blue ellipse indicates the approximate region within which dextral shear is accommodated by bookshelf slip. (b) Fault-normal velocities projected onto a line (gold) approximating the fault trajectory in a direction parallel to the motion on the SAF (azimuth 138°). (c) Transverse velocities projected as in (b). (d) Transverse velocity distribution across the WTR. See text for discussion.

rotated to $<45^\circ$ to the SAF they became reactivated in a dextral sense.

Our calculated rate of stretching along the WTR is quite large, and raises questions about how it is accommodated. Possibilities include conjugate or single sets of small-scale strike-slip faults oblique to the trend of the WTR, or normal faults at a high angle to the WTR.

No variation in tangential velocities normal to the fault is detectable above the noise level (Fig. 4d), indicating a lack of elastic strain accumulation associated with the strike-slip faults of the WTR. This is consistent with the current low rate of strike-slip predicted by our analysis.

Our calculated rotation rate of 1.6° Myr^{-1} is significantly less than the long-term rotation rate of $\sim 5^\circ$ Myr^{-1} (Jackson & Molnar 1990). This is because the faults in the WTR have been rotated into a relatively low angle to the trend of the SAF, progressively reducing the rate of rotation. At the present rate of dextral shear across the WTR, the rotation rate would be 3.8° Myr^{-1} if the faults were at 90° to the trend of the SAF, and displacement rates through the Borderland may have been higher in the past. Our calculated rate is nearly twice the value determined by McCaffrey (2005) from the geodetic data (0.9°Myr^{-1}), however. This is because the sum total of all the components of deformation in the WTR (slip on the faults, fault-normal shortening, fault-parallel extension and rotation) is equivalent to dextral simple shear parallel to the SAF, so that the rotation is difficult to detect directly. McCaffrey (2005) makes the point that transverse components of velocity (normal to the transform trend) are very small, and bases his estimate of the rotation rates on that. This approach correctly limits the amount of rigid body rotation of the Transverse Ranges as a whole, but it does not limit rotations of the faults produced by the mechanism discussed here, in which other components of deformation are involved.

5 COMPARISON WITH OTHER MODELS

We propose in this paper that the bookshelf slip model can explain three distinctive features of the left-lateral faults and fault panels in the San Andreas Transform system: (1) the lack of a geodetic signature of slip on left-lateral faults that are known to be active; (2) the lack of a geodetic signature of rotation, in contrast to the palaeomagnetic evidence and (3) the distinctive way in which NW-trending right-lateral faults forming part of the transform system lose displacement and die out as they approach the left-lateral faults. What are the alternative hypotheses, and how do they compare in their ability to explain these features?

Analyses based on elastic dislocation theory commonly fail to recognize either the slip on the left-lateral faults or the vertical-axis rotation. Savage *et al.* (2001) concluded from analysis of GPS and trilateration data that there is no measurable slip rate on the Garlock Fault, in contrast to the geological estimates of active slip at rates up to 11 mm yr^{-1}. They suggested that the Garlock Fault is rotating, based on the rate of shear in the ECSZ, but did not invoke the bookshelf slip model. Block models using elastic dislocation theory also tend to underestimate the slip rates on the left-lateral faults: Meade & Hager (2005) and Becker *et al.* (2005) estimate slip rates on the Garlock Fault at 1.1–3.2 and 3.1 ± 10 mm yr^{-1}, respectively. The problem is most clearly demonstrated by McCaffrey (2005), who used an elastic block model to analyse deformation in the SW United States. He concluded that vertical-axis rotation in the WTR is $\sim 0.9^\circ$ Myr^{-1}, which is not distinguishable within error from the rotation of the Pacific Plate. This contrasts with the long-term rotation rate of $\sim 5^\circ$ Myr^{-1} determined from palaeomagnetic measurements, and our own determination of 1.6° Myr^{-1} for the present-day rate.

Spinler *et al.* (2010) carried out a very detailed analysis of deformation in the eastern Transverse Ranges (Joshua Tree area) using elastic block models to analyse new campaign-style GPS data. They compared four different models for the area, incorporating varying amounts of vertical-axis rotation from zero to 15° Myr^{-1}, which were to a large extent specified by the chosen block geometry. The models involving rotation are, in effect, bookshelf slip or 'transrotation' models. They concluded that the models cannot be distinguished from each other in terms of how well they fit the observed geodetic velocities and the geological measurements of slip rate and rotation on the faults. Their analysis is in effect an elaborate demonstration of the point made earlier in this paper, that the bookshelf slip process cannot easily be recognized from geodetic data alone.

Viscoelastic block models provide a much greater degree of flexibility in interpreting the geodetic data. By varying the time in the viscoelastic earthquake cycle, a wide variety of velocity profiles can be obtained for a given slip rate on a fault. Chuang & Johnson (2011), for example, were able to fit the velocity data around the Garlock Fault with a slip rate of 11 mm yr^{-1}, by assuming that the fault is very late in a very long viscoelastic cycle (5000 yr). The solution is not unique, however: as we point out, the data can also be fit by assuming creep on the fault at 1 mm yr^{-1}. Viscoelastic block models also tend to produce low estimates for vertical-axis rotation. Hammond *et al.* (2011), in their analysis of deformation in the Walker Lane, predict a vertical-axis rotation of 1.3° Myr^{-1} for the fault blocks bounded by the left-lateral Carson and Ollinghouse lineaments, in contrast to the palaeomagnetic evidence for long-term rotation rates of 3–5° Myr^{-1}. These lineaments trend at $\sim 90^\circ$ to the right-lateral faults in the ECSZ, which in that area has a slip rate of around 7 mm yr^{-1} distributed across a zone $\sim$150 km wide. The bookshelf slip model would therefore predict a rotation rate for the fault blocks of $\sim 2.7^\circ$ Myr^{-1}. This is closer to the long-term rotation rate than that predicted by the viscoelastic block model.

6 CONCLUSIONS

Bookshelf slip is difficult to detect geodetically, because rotation of the fault panel cancels out the velocity signal of the slip, and the combination of slip and rotation is kinematically equivalent to bulk shear at an angle to the slipping faults. This explains why a number of geodetic studies have concluded that the faults have negligible slip rates, and that they are not rotating. We show that the rate of dextral shear in the ECSZ is consistent with a sinistral slip rate of 6 mm yr^{-1} on the central section of the Garlock Fault, and a clockwise rotation rate of 4° Myr^{-1} for the fault and its surroundings. The rotation of the fault can be measured directly from the gradient in the fault-normal component of motion. The only direct indication of slip on the fault, however, may be the residual elastic flexure across the fault. The pattern of transverse velocities on either side of the Garlock Fault is consistent with the elastic flexure expected for our predicted slip rate, but the signal is small compared to the noise in the data, and other interpretations are possible.

The WTR provide an example of a panel of sinistral faults that have rotated into an orientation such that they are now being reactivated as dextral faults with a very slow cumulative slip rate. The velocity field is consistent with a clockwise rotation rate of 1.6° Myr^{-1}, and with as much as 6 mm yr^{-1} extension parallel to the trend of the ranges.

ACKNOWLEDGEMENTS

This research was supported by the Southern California Earthquake Center (SCEC). SCEC is funded by National Science Foundation Cooperative Agreement EAR-0529922 and United States Geological Survey Cooperative Agreement 07HQAG0008. The SCEC contribution number for this paper is 1531. We thank EarthScope PBO as well as Corné Kreemer, William Hammond and their contributors for openly sharing geodetic data products, and George Hilley and an anonymous reviewer, as well as the associate editor, for their constructive comments on the manuscript.

REFERENCES

Barbot, S. & Fialko, Y., 2010. A unified continuum representation of post-seismic relaxation mechanisms: semianalytic models of afterslip, poroelastic rebound and viscoelastic flow, *Geophys. J. Int.,* **182,** 1124–1140.

Becker, T.W., Hardebeck, J.L. & Anderson, G., 2005. Constraints on fault slip rates of the southern California plate boundary from GPS velocity and stress inversions, *Geophys. J. Int.,* **160,** 634–650.

Bennett, R.A., Wernicke, B.P., Niemi, N.A., Friedrich, A.M. & Davis, J.L., 2003. Contemporary strain rates in the northern Basin and Range province from GPS data, *Tectonics,* **22,** 1008, doi:10.1029/2001TC001355.

Bird, P., 2009. Long-term fault slip rates, distributed deformation rates, and forecast of seismicity in the western United States from joint fitting of community geologic, geodetic, and stress direction data sets, *J. geophys. Res.,* **114,** B11403, doi:10.1029/2009JB006317.

Carter, J.N., Luyendyk, B.P. & Terres, R., 1987. Neogene clockwise tectonic rotation of the eastern Transverse Ranges, California, suggested by paleomagnetic vectors, *Bull. geol. Soc. Am.,* **98,** 199–206.

Cashman, P.H. & Fontaine, S.A., 2000. Strain partitioning in the northern Walker Lane, western Nevada and northeastern California, *Tectonophysics,* **326,** 111–130.

Chuang, R.Y. & Johnson, A.M., 2011. Reconciling geologic and geodetic model fault slip-rate discrepancies in southern California: consideration of nonsteady mantle flow and lower crustal fault creep, *Geology,* **39,** 627–630.

Cowan, D.S., Botros, M. & Johnson, H.P., 1986. Bookshelf tectonics: rotated crustal blocks within the Sovanco Fracture Zone, *Geophys. Res. Lett.,* **13,** 995–998.

Davis, G.A. & Burchfiel, B.C., 1973. Garlock Fault: an intracontinental transform structure, southern California, *Bull. geol. Soc. Am.* , **84,** 1407–1422.

Freed, A.M., Hirth, G. & Behn, M.D., 2012. Using short-term postseismic displacements to infer the ambient deformation conditions of the upper mantle, *J. geophys. Res.,* **117,** B01409, doi:10.1029/2011JB008562.

Giorgis, S., Markley, M. & Tikoff, B., 2004. Vertical-axis rotation of rigid crustal blocks driven by mantle flow, in *Vertical Coupling and Decoupling in the Lithosphere,* Vol. **227,** pp. 83–100, eds Grocott, J., McCaffrey, K.J.W., Taylor, G. & Tikoff, B., Geological Society of London Special Publication.

Hammond, W.C., Blewitt, G. & Kreemer, C., 2011. Block modeling of crustal deformation of the northern Walker Lane and Basin and Range from GPS velocities, *J. geophys. Res.,* **116,** B04402, doi:10.1029/2010JB007817.

Jackson, J. & Molnar, P., 1990. Active faulting and block rotations in the western Transverse Ranges, California, *J. geophys. Res.,* **95,** 22 073–22 087.

Kreemer, C. & Hammond, W.C., 2007. Geodetic constraints on areal changes in the Pacific-North America plate boundary zone: what controls Basin and Range extension? *Geology,* **10,** 943–947.

Lamb, S., 1987. A model for tectonic rotations about a vertical axis, *Earth planet. Sci. Lett.,* **84,** 75–86.

Luyendyk, B.P., Kamerling, M.J. & Terres, R., 1980. Geometric model for Neogene crustal rotations in southern California, *Bull. geol. Soc. Am.,* **91,** 211–217.

McCaffrey, R., 2005. Block kinematics of the Pacific–North American plate boundary in the southwestern United States from inversion of GPS, seismological, and geologic data, *J. geophys. Res.,* **110,** B07401, doi:10.1029/2004JB003307.

McClusky, S.C., Bjornstad, S.C., Hager, B.H., King, R.W., Meade, B.J., Miller, M.M., Monastero, F.C. & Souter, B.J., 2001. Present day kinematics of the eastern California shear zone from a geodetically constrained block model, *Geophys. Res. Lett.,* **28,** 3369–3372.

McGill, S.F., Wells, S.G., Fortner, S.K., Kuzma, H.A. & McGill, J.D., 2009. Slip rate of the western Garlock fault, at Clark Wash, near Lone Tree Canyon, Mojave Desert, California, *Bull. geol. Soc. Am.,* **121,** 536–554.

McKenzie, D.P. & Jackson, J., 1983. The relationship between strain-rates, crustal thickening, palaeomagnetism, finite strain and fault movements within a deforming zone, *Earth planet. Sci. Lett.,* **65,** 182–202.

Meade, B.J. & Hager, B.H., 2005. Block models of crustal motion in southern California constrained by GPS measurements, *J. geophys. Res.,* **110,** B03403, doi:10.1029/2004JB003209.

Onderdonk, N.W., 2005. Structures that accommodated differential vertical axis rotation of the western Transverse Ranges, California, *Tectonics,* **24,** TC4018, doi:10.1029/2004TC001769.

Oskin, M. & Iriondo, A., 2004. Large magnitude transient strain accumulation on the Blackwater fault, eastern California shear zone, *Geology,* **32,** 313–316.

Platt, J.P. & Becker, T.W., 2010. Where is the real transform boundary in California? *Geochem. Geophys. Geosyst.,* **11,** Q06012, doi:10.1029/2010GC003060.

Pollitz, F.F., McCrory, P., Svarc, J. & Murray, J., 2008. Dislocation models of interseismic deformation in the western United States, *J. geophys. Res.,* **113,** B04413, doi:10.1029/2007JB005174.

Savage, J. & Burford, R., 1973. Geodetic determination of relative plate motion in central California, *J. geophys. Res.,* **78,** 832–845.

Savage, J.C., Gan, W. & Svarc, J.L., 2001. Strain accumulation and rotation in the eastern California shear zone, *J. geophys. Res.,* **106,** 21 995–22 007.

Schermer, E.R., Luyendyk, B.P. & Cisowski, S., 1996. Late Cenozoic structure and tectonics of the northern Mojave Desert, *Tectonics,* **15,** 905–932.

Spinler, J.C., Bennett, R.A., Anderson, M.L., McGill, S., Hreinsdottir, S. & McCallister, A., 2010. Present-day strain accumulation and slip rates associated with southern San Andreas and eastern California shear zone faults, *J. geophys. Res.,* **115,** B11407, doi:10.1029/2010JB007424.